

NOVEL TILE SEGMENTATION SCHEME FOR OMNIDIRECTIONAL VIDEO

Jisheng Li, Ziyu Wen, Sihan Li, Yikai Zhao, Bichuan Guo, Jiangtao Wen

Tsinghua University
Beijing, 100084, China

ABSTRACT

Regular omnidirectional video encoding technics use map projection to flatten a scene from a spherical shape into one or several 2D shapes. Common projection methods including equirectangular and cubic projection have varying levels of interpolation that create a large number of non-information-carrying pixels that lead to wasted bitrate. In this paper, we propose a tile based omnidirectional video segmentation scheme which can save up to 28% of pixel area and 20% of BD-rate averagely compared to the traditional equirectangular projection based approach.

Index Terms— Omnidirectional video, tile segmentation

1. INTRODUCTION

The ever wider application of virtual reality (VR) requires that omnidirectional video for consumption on VR devices be efficiently captured, encoded and transmitted.

Various types of equipment for recording omnidirectional video has already been developed. Most of these capturing equipments use two fish-eye cameras or multiple wide angle cameras to capture the scene and then stitch frames from these cameras together. In this process, an omnidirectional picture well represented using a spherical surface is created, and then mapped into a flat plane for subsequent encoding and then transmitted. A number of mapping methods from the spherical to flat surfaces have been proposed, such as the technique in [1] [2] [3], with various distortions created during the process [4].

In this paper, we propose a tile-based segmentation and projection scheme. It attempts to create an approximate equal-area mapping and projection with compression-friendly shapes with less wasteful pixels. Our scheme can save up to 28% of pixel area compare to equirectangular projection and 40% of pixel area compare to cubic [5] projection at the same minimum sampling density in the original spherical surface.

The paper is organized as follows: In section 2, we review related work and the quality metric. Section 3 describes the proposed tile segmentation scheme in details. Experimental results are shown in section 4 while section 5 is the conclusion.

2. RELATED WORK

Many early techniques for capturing omnidirectional video [6] [7] used a camera and a parabolic mirror. The camera captures images reflected by the parabolic mirror, with the vertical field of view limited in 90° .

Lately, higher quality omnidirectional video are captured with multiple high definition cameras with the captured frames stitched [8]. When projecting the image to a flat 2D plane, equirectangular projection was widely used. Despite of its ease of use, because the

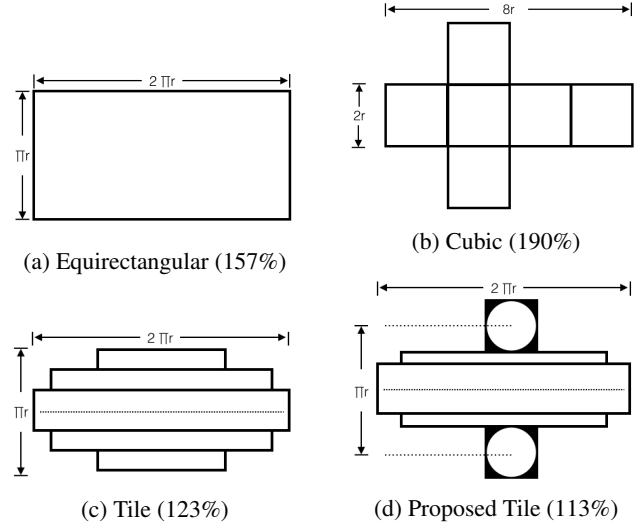


Fig. 1. Comparison of map projections under same minimum sample density on the sphere (with percentage of original sphere area in the brackets). (c) A tile segmentation scheme with equal division on latitude; (d) Our proposed 5-tiles scheme

areas in the north and south poles of the sphere are stretched more severely than areas near the equator, overall, a net increase of 57% of the original sphere area was introduced wastefully, leading to a resultant increase in bitrate. Furthermore, due to the distortions introduced by the stretching, especially near the two poles, predictive coding tools in video encoders fail more easily, causing further reduction in coding efficiency.

In [5], Ng et al. proposed a method to project a sphere onto a cube, referred as cubic projection subsequently. Although the distortion introduced by projection is mitigated in cubic projection, the total area of the 6 sides has to be 190% of the original sphere area so that the central of each surface has enough sample density, as is shown in Fig.1. Later in [9], Fu et al. proposed a rhombic dodecahedron map projection scheme, which divided a sphere into 12 rhombs then reshape to squares and rearrange into a rectangular.

In [10], Yu et al. divided the video vertically into tiles and resized the tiles according to the latitudes or user preferences (e.g. areas near the poles might be less likely to be requested by the viewer). Even though this scheme solved many of the issues caused by stretch related distortions and increase in the total number of pixels after mapping, it did not fully address the issue of preserving effectiveness of predictive coding tools in video encoders.

There are relatively few studies on methods for evaluating video

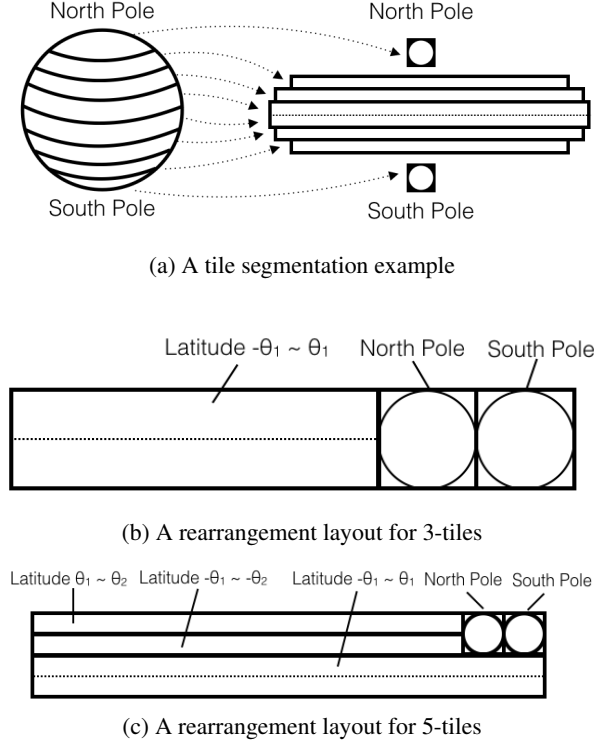


Fig. 2. Tile segmentation and rearrangement illustration

coding quality for omnidirectional video. Such evaluation is a challenge because after the input omnidirectional video is projected onto a 2D plane and then coded, many of the pixels in the resulted video may be interpolated and should not carry the same “weight” as in regular PSNR calculation. In [11], Yu et al. proposed two sphere-based PSNR computations, named S-PSNR and L-PSNR respectively. The S-PSNR weights all position on the sphere equally while the L-PSNR weights positions according to their latitudes and access frequency. In this paper, we use these two metrics to measure the quality of encoded video in Section 4 and used L-PSNR to replace regular PSNR in the BD-Rate calculations.

3. TILE SEGMENTATION SCHEME

We start by analyzing the equirectangular projection and striving to minimize the pixel area after the projection. We divide a sphere into several pieces along latitude lines into two camber surfaces and rings, flatten the camber surfaces into circles and cut open the rings, and then unfold and reshape them into rectangular tiles. Finally, we expand the two circles corresponding to the north and south poles of the original sphere to their bounding square with a black filling, as shown in Fig.2(a). The resulted tiles are still approximately equal in size.

Following these steps, with the number of titles increasing, the afore-described mapping will create a set of approximately equal-area titles with the total area approaching the that of the original sphere.

3.1. Area comparison

The total area of each hemisphere’s tiles can be describe as:

$$S_{hemisphere} = S_{pole} + \sum_{i=1}^n 2\pi r^2 \cos \theta_{i-1} (\theta_i - \theta_{i-1}). \quad (1)$$

$$S_{pole} = \begin{cases} \pi(\frac{\pi}{2} - \theta_p)^2 r^2 & , \text{Circle Pole} \\ 4(\frac{\pi}{2} - \theta_p)^2 r^2 & , \text{Square Pole} \end{cases} \quad (2)$$

where $\theta_1, \theta_2 \dots \theta_n$ are the latitude (in rad) of the borders, e.g. for north hemisphere $\theta_1, \theta_2 \dots \theta_n \in (0, \frac{\pi}{2})$ and $\theta_1 < \theta_2 < \dots < \theta_n = \theta_p$. $\theta_0 = 0$ corresponds to the latitude of the equator, while θ_p is the latitude of the outer edge of the pole areas which is actually the same with θ_n . After n cuts at each hemisphere, the sphere is projected and divided into $(2n + 1)$ tiles, with one big tile across the equator.

In the tile segmentation method proposed in Yu’s work[10], the area of pole under same minimum sample density is

$$S_{pole, Yu} = 2\pi r^2 (\frac{\pi}{2} - \theta_p) \cos \theta_p. \quad (3)$$

which is always larger than Eq.2.

The best segmentation scheme can be found by minimizing the total area given a number of the tiles n :

$$\Theta_n = \{\theta_1, \dots, \theta_n\} = \arg \min_{0 < \theta_1 < \dots < \theta_n < \frac{\pi}{2}} S_{hemisphere}. \quad (4)$$

Some of the best schemes are shown in Fig.3 and Table 1, where the results with the pole areas calculated as circles or black-filled to bounding boxes (2) are marked with circles and *Circle Poles*, or crosses and *Square Poles*. The horizontal axis in the figure is the number of cuts in each hemisphere, while the vertical axis shows the area as a ratio with regard to the area of the original sphere.

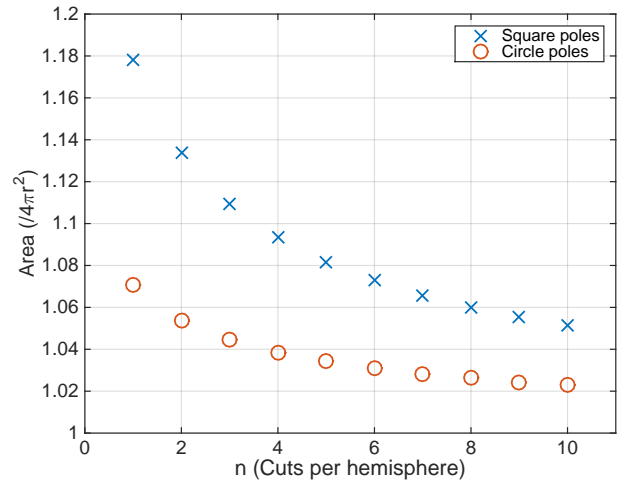


Fig. 3. Relation between cut number and total area without overlap

Fig.3 shows that increasing the number of tiles can effectively reduce the total area. It is of interest to note that when the number of tiles becomes very large, the corresponding tile based segmentation becomes the equal-area sinusoidal projection.

In practice however, the number of tiles is limited by the overhead introduced by using tile-based video coding (when each tile is encoded independently) as well as the capability of the decoder to decode video encoded with multiple titles.

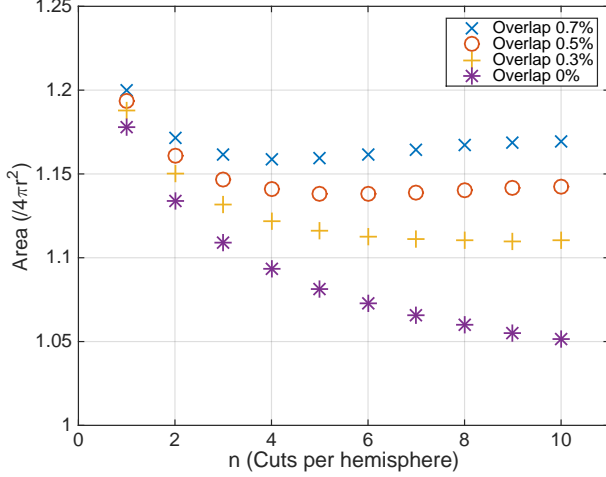


Fig. 4. Total area comparison of different tile number and overlap (Square poles)

3.2. Overlapping

When a tiled video is encoded at a low bitrate, border artifacts exist between tile boundaries. A common approach to this issue is to set overlapping areas between tiles.

Introducing overlaps will increase the total area. Hence the optimization problem in (4) becomes:

$$S_{hemisphere}(\sigma) = S_{pole}(\sigma) + 2\pi r^2 \left(\theta_1 + \frac{\sigma\pi}{2} \right) + \sum_{i=2}^n 2\pi r^2 \cos \theta_{i-1} (\theta_i - \theta_{i-1} + \sigma\pi). \quad (5)$$

$$S_{pole}(\sigma) = \begin{cases} \pi \left(\frac{\pi}{2} - \theta_p + \frac{\sigma\pi}{2} \right)^2 r^2 & , \text{Circle Pole} \\ 4 \left(\frac{\pi}{2} - \theta_p + \frac{\sigma\pi}{2} \right)^2 r^2 & , \text{Square Pole} \end{cases} \quad (6)$$

$$\Theta_{n,\sigma} = \{\theta_1, \dots, \theta_n\} = \arg \min_{\frac{\sigma\pi}{2} < \theta_1 < \dots < \theta_n < \frac{\pi - \sigma\pi}{2}} S_{hemisphere}(\sigma). \quad (7)$$

$$\Theta_\sigma = \arg \min_{\Theta_{n,\sigma}} S_{hemisphere}(\sigma). \quad (8)$$

where Θ_σ is the optimization result, and σ is the percentage of the overlap in height, e.g. 0.5% overlap of a 1080p video is 5 pixel width. Some of the solutions to the optimization problem are shown in Fig.4 and Table 1. For the same overall area, the increase of the overlapped areas will reduce the number of tiles, from 41-tiles at 0.1% overlap to 9-tiles at 0.7% overlap.

3.3. Rearrangement and layout

When some decoders can not decode multiple streams at the same time, compacting all the tiles into one rectangular video stream is needed for compatibility.

Fig. 2 (b) and (c) are examples of such layout transforming multiple tiles into a single rectangular tile. As the number of tiles increases, more pixels will be wasted due to layout overhead. It's worth noting that the layout in Fig.2 (b) with segmentation at $\theta_1 = 45^\circ$ is the optimum for 3-tiles, from both layout and sample density (shown in Table 1) aspect.

Table 1. Optimization results on specified tiles number and overlap percentage (in degrees)

Scheme	0% overlap	0.3% overlap	0.5% overlap
3-tiles			
(Circle pole)	$\theta_1=32.70^\circ$	$\theta_1=32.97^\circ$	$\theta_1=33.15^\circ$
5-tiles			
(Circle pole)	$\theta_1=25.34^\circ$ $\theta_2=38.22^\circ$	$\theta_1=26.08^\circ$ $\theta_2=38.81^\circ$	$\theta_1=26.58^\circ$ $\theta_2=39.21^\circ$
3-tiles			
(Square pole)	$\theta_1=45.00^\circ$	$\theta_1=45.27^\circ$	$\theta_1=45.45^\circ$
5-tiles			
(Square pole)	$\theta_1=35.07^\circ$ $\theta_2=53.17^\circ$	$\theta_1=35.81^\circ$ $\theta_2=53.77^\circ$	$\theta_1=36.30^\circ$ $\theta_2=54.18^\circ$

4. EXPERIMENTAL RESULTS

4.1. Non-overlapping RD performance

The RD performance experiments were conducted with the widely used open source HEVC encoder x265[12] on its default settings. The test sequences are from two datasets. The first 10 sequences in Table 2 and Table 3 are 9K images from SUN360 database[13], and the last two sequences are 4K video clips generously provided by LETINVR.

The QPs used for computing the BD-rate are 22, 27, 32, 37. For the quality metric, we use the S-PSNR and L-PSNR as in [11] and introduced in Section 2. The S-PSNR weights all position on the sphere equally while the L-PSNR weights positions according to its latitude access frequency. In our experiments, we measured both metrics and we used both S-PSNR and L-PSNR in the BD-Rate calculations.

As the test sequences are all in equirectangular projection format as ground truth, we down-sampled the sequences in the experiments so that the ground truth has always higher sample density. For example, the SUN360 experiments were conducted at 4552x2276 while the inputs are at 9104x4552 equirectangular. When calculating S-PSNR and L-PSNR, decoded sequences were mapped back to equirectangular with the original input resolution. Bilinear interpolation was used in above steps.

The experiment results are shown in Fig.5, Table 2 and Table 3, including proposed 3-tiles scheme (P3), proposed 5-tiles scheme (P5), cubic projection (CP). In [10], Yu et al. proposed a tile segmentation method and here we implement it as 3-tiles (Y3) and 5-tiles (Y5).

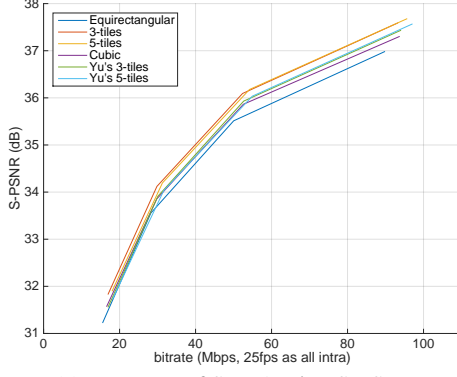
Table 2 and 3 show about 12% and 20% bitrate savings to equirectangular projection on S-PSNR and L-PSNR respectively, which are 4% and 6% more compared to the previous method.

4.2. Overlapping de-blocking performance

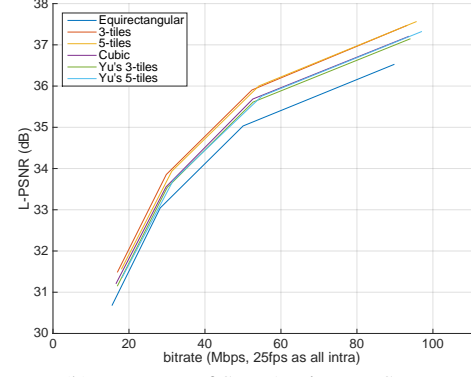
In this section we compare the non-overlapped and different percentage overlapped result with 3-tiles and 5-tiles configuration. The output sequence was encoded with QP 22, 27, 32, 37 and different overlap configuration, then decoded and blended the overlapping area.

The third row in Fig.6, shows the de-blocking result of 0.5% overlap, which gives a well enough transition. For a 4k video, 0.5% overlap costs 10 pixel width.

The BD-rate results of proposed 3-tiles and 5-tiles scheme with 0.5% overlap compared to non-overlap is shown in Table 4, where such overlap scheme introduces no more than 1.7% bitrate overhead averagely.



(a) RD curve of Seq. 1 using S-PSNR



(b) RD curve of Seq. 1 using L-PSNR

Fig. 5. RD curves of two sequences with S-PSNR and L-PSNR metric.

Table 2. BD-Rate of proposed method using S-PSNR

Seq.	P3	P5	CP	Y3	Y5
1	-11.6%	-9.8%	-4.6%	-5.5%	-4.5%
2	-13.1%	-13.4%	-9.2%	-10.2%	-10.4%
3	-12.5%	-11.8%	-12.2%	-7.4%	-7.5%
4	-10.6%	-10.0%	-7.3%	-6.8%	-7.2%
5	-15.2%	-16.4%	-10.3%	-12.3%	-12.9%
6	-8.0%	-14.7%	-3.1%	-7.5%	-7.7%
7	-12.9%	-13.1%	-8.2%	-10.3%	-11.0%
8	-8.4%	-7.0%	-1.4%	-4.5%	-3.9%
9	-1.4%	1.0%	1.2%	0.9%	2.8%
10	-13.7%	-13.4%	-9.6%	-9.7%	-10.9%
11	-16.8%	-18.6%	-0.4%	-11.3%	-14.6%
12	-22.5%	-23.9%	-7.8%	-13.6%	-17.5%
Avg.	-12.2%	-12.6%	-6.1%	-8.2%	-8.8%

Table 3. BD-Rate of proposed method using L-PSNR

Seq.	P3	P5	CP	Y3	Y5
1	-18.5%	-17.5%	-11.8%	-10.0%	-10.3%
2	-17.9%	-18.3%	-12.3%	-13.6%	-14.7%
3	-19.7%	-19.2%	-18.8%	-12.2%	-13.2%
4	-19.8%	-19.3%	-17.3%	-11.3%	-12.9%
5	-24.6%	-25.0%	-22.1%	-16.2%	-17.8%
6	-20.4%	-19.9%	-18.7%	-12.7%	-14.4%
7	-27.6%	-27.0%	-24.7%	-16.9%	-19.5%
8	-16.4%	-15.5%	-9.7%	-8.5%	-9.0%
9	-10.6%	-8.3%	-7.4%	-4.2%	-3.6%
10	-21.7%	-21.3%	-10.0%	-13.8%	-16.2%
11	-22.5%	-23.9%	-7.8%	-24.1%	-23.9%
12	-21.9%	-21.0%	-5.0%	-11.9%	-13.1%
Avg.	-20.1%	-19.7%	-14.6%	-13.0%	-14.1%

Table 4. BD-rate result of 0.5% overlap compare to 0% overlap

Seq.	S-PSNR		L-PSNR	
	P3	P5	P3	P5
1	0.8%	1.2%	0.9%	1.4%
2	1.4%	0.4%	1.6%	0.4%
3	0.9%	2.3%	0.8%	2.2%
4	1.0%	1.4%	1.1%	1.6%
5	1.0%	1.9%	1.1%	1.9%
6	1.1%	2.3%	1.3%	2.6%
Avg.	1.0%	1.6%	1.1%	1.7%

Overlap

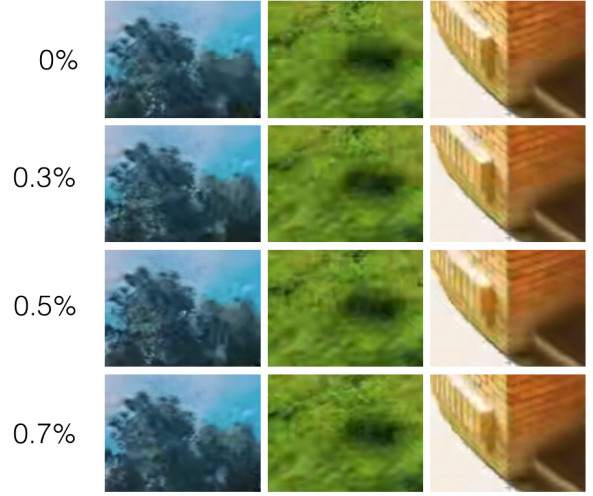


Fig. 6. Comparison on the border of tile with 0%, 0.3%, 0.5% and 0.7% overlap from top to bottom, QP = 37.

5. CONCLUSION

In this paper, we proposed a tile segmentation scheme for omnidirectional video encoding, which has less pixel wastage and more legitimate mapping method. Experimental results show the proposed scheme can save up to 28% of pixel area and 20% BD-rate averagely compare to traditional equirectangular projection.

Future work includes optimization on segmentation scheme targeting on region of interest (ROI) application, as well as optimizations on temporal and spacial random access.

6. REFERENCES

- [1] John P Snyder, *Flattening the earth: two thousand years of map projections*, University of Chicago Press, 1997.
- [2] Shenchang Eric Chen, "Quicktime vr: An image-based approach to virtual environment navigation," in *Proceedings of*

the 22nd annual conference on Computer graphics and interactive techniques. ACM, 1995, pp. 29–38.

- [3] Richard Szeliski and Heung-Yeung Shum, “Creating full view panoramic image mosaics and environment maps,” in *Proceedings of the 24th annual conference on Computer graphics and interactive techniques*. ACM Press/Addison-Wesley Publishing Co., 1997, pp. 251–258.
- [4] Denis Zorin and Alan H Barr, “Correction of geometric perceptual distortions in pictures,” in *Proceedings of the 22nd annual conference on Computer graphics and interactive techniques*. ACM, 1995, pp. 257–264.
- [5] King-To Ng, Shing-Chow Chan, and Heung-Yeung Shum, “Data compression and transmission aspects of panoramic videos,” *Circuits and Systems for Video Technology, IEEE Transactions on*, vol. 15, no. 1, pp. 82–95, 2005.
- [6] Ivana Tošić and Pascal Frossard, “Low bit-rate compression of omnidirectional images,” in *Picture Coding Symposium, 2009. PCS 2009*. IEEE, 2009, pp. 1–4.
- [7] Ingo Bauermann, Matthias Mielke, and Eckehard Steinbach, “H. 264 based coding of omnidirectional video,” in *Computer Vision and Graphics*, pp. 209–215. Springer, 2006.
- [8] Patrice Ronda Alface, Jean-François Macq, and Nico Verzijp, “Interactive omnidirectional video delivery: A bandwidth-effective approach,” *Bell Labs Technical Journal*, vol. 16, no. 4, pp. 135–147, 2012.
- [9] Chi-Wing Fu, Liang Wan, Tien-Tsin Wong, and Chi-Sing Leung, “The rhombic dodecahedron map: An efficient scheme for encoding panoramic video,” *Multimedia, IEEE Transactions on*, vol. 11, no. 4, pp. 634–644, 2009.
- [10] Matt Yu, Haricharan Lakshman, and Bernd Girod, “Content adaptive representations of omnidirectional videos for cinematic virtual reality,” in *Proceedings of the 3rd International Workshop on Immersive Media Experiences*. ACM, 2015, pp. 1–6.
- [11] Matt Yu, Haricharan Lakshman, and Bernd Girod, “A framework to evaluate omnidirectional video coding schemes,” in *Mixed and Augmented Reality (ISMAR), 2015 IEEE International Symposium on*. IEEE, 2015, pp. 31–36.
- [12] “x265,” <http://x265.org>.
- [13] Jianxiong Xiao, Krista A Ehinger, Aude Oliva, and Antonio Torralba, “Recognizing scene viewpoint using panoramic place representation,” in *Computer Vision and Pattern Recognition (CVPR), 2012 IEEE Conference on*. IEEE, 2012, pp. 2695–2702.